



## OPEN ACCESS

## EDITED BY

Qiushi Huang,  
Tongji University, China

## REVIEWED BY

Riccardo Signorato,  
S.R.I. Tech s.r.l., Italy  
Simon Alcock,  
Diamond Light Source, United Kingdom  
Yong Wang,  
Shanghai Advanced Research Institute  
(CAS), China  
Maurizio Vannoni,  
European X-Ray Free Electron Laser,  
Germany

## \*CORRESPONDENCE

Fugui Yang,  
yangfg@ihep.ac.cn

## SPECIALTY SECTION

This article was submitted to Optics and  
Photonics,  
a section of the journal  
Frontiers in Physics

RECEIVED 07 April 2022

ACCEPTED 04 August 2022

PUBLISHED 28 September 2022

## CITATION

Hu W, Cui X, Li M, Sheng W, Zhang W,  
Jia Q and Yang F (2022), Study on the X-  
ray mirror quality specification in  
advanced light source.  
*Front. Phys.* 10:915182.  
doi: 10.3389/fphy.2022.915182

## COPYRIGHT

© 2022 Hu, Cui, Li, Sheng, Zhang, Jia  
and Yang. This is an open-access article  
distributed under the terms of the  
Creative Commons Attribution License  
(CC BY). The use, distribution or  
reproduction in other forums is  
permitted, provided the original  
author(s) and the copyright owner(s) are  
credited and that the original  
publication in this journal is cited, in  
accordance with accepted academic  
practice. No use, distribution or  
reproduction is permitted which does  
not comply with these terms.

# Study on the X-ray mirror quality specification in advanced light source

Weishan Hu<sup>1,2</sup>, Xiaowen Cui<sup>1,2</sup>, Ming Li<sup>1,2</sup>, Weifan Sheng<sup>1,2</sup>,  
Weiwei Zhang<sup>1</sup>, Quanjie Jia<sup>1</sup> and Fugui Yang<sup>1\*</sup>

<sup>1</sup>Beijing Synchrotron Radiation Facility, Institute of High Energy Physics, Chinese Academy of Science, Beijing, China, <sup>2</sup>University of Chinese Academy of Sciences, Beijing, China

The influence of the X-ray mirror errors on the performance of the beamline increases as the X-ray beam's coherence improves in advanced light sources. The spatial dispersion of the X-ray beam is crucial for spatial resolution and field of view. However, selecting the appropriate merit function for expressing light distribution and identifying its relationship to optical error is very important in beamline design. We develop a high-efficiency wave-optics simulation platform and a deterministic analysis model to address this issue. The simulation experiments evaluated merit functions, including Strehl ratio, root-mean-square spot size, and encircled energy radius. We proved that the encircled energy radius is a good metric of the x-ray beam spatial dispersion, which matches the results of the Church-Takacs theory. In addition, it is found that limiting the contribution of the low frequency ( $wavelength > \frac{1}{10} L$ ) error is effective for specifying the requirements of X-ray mirrors.

## KEYWORDS

X-ray mirror, beamline design, simulation, surface error, synchrotron radiation facility

## Introduction

X-rays emitted by advanced light sources, including free-electron lasers (FELs) and synchrotron radiation facilities, have advantages such as high flux and brightness. The fourth-generation synchrotron radiation source can achieve sub-micron spatial resolution. It can be used in many applications such as materials science, spectroscopy, chemistry, biology, etc. However, due to the high coherence of X-rays, various optical devices and equipment of beamlines will cause wavefront errors, which will reduce the system's spatial resolution or the peak intensity of beams. Therefore, these advantages of synchrotron radiation make high demands on optics quality for beamline transmission. For example, the surface shape accuracy of the High Energy Photon Source (HEPS)[1] for the X-ray nano-focusing mirror is required up to 2 nm peak-to-value (PV) or 0.5 nm root-mean-square (RMS), and the slope error is required to be better than 50  $\mu rad$  RMS.

The influence of X-ray mirror shape errors have always been an essential issue in synchrotron radiation facilities. X-ray optical elements' specifications have been studied

over the past few years. Church and Takacs [2] performed a systematic analysis of the errors of optical focusing elements as early as 1993, and they used the error statistics of the focusing elements to predict the imaging degradation of simple imaging systems. Church's article presents a model of errors and proposes two types of error, including the figure error left by the molding process during manufacturing and the finish error left by the finishing and polishing process. At the same time, R. Signorato and M. Sanchez del Rio [3] researched X-ray mirrors based on geometric ray tracing. They proposed that the power spectral density (PSD) does not contain all the information about the intensity and position of the light spot. On this basis, Pardini [4] finds that for diffraction-limited systems, within a critical spatial wavelength, the optical focusing element can appropriately relax the slope error requirements and still maintain a good light intensity distribution. Yashchuk [5] studied the effect of the specular error on the quality of the X-ray beam delivered to the sample location at different spatial frequencies. It shows that for a surface irregularity comparable to the mirror length, a significantly reduced photon flux density results in reduced beam quality. On the basis of the theoretical model, the power spectral density function [6–8], surface finish function [9,10] can be used to express the specific requirements of X-ray optical components.

According to the requirements for the manufacturing parameters of optical elements, adequate progress has also been made in manufacturing high-precision optical elements. Many researchers [11,12] have investigated high-precision optical components suitable for X-rays. But inevitably, high-precision optical components are expensive and difficult for manufacture. Also, not all experiments require highly coherent or diffraction-limited light, which means imperfect mirrors can suffice for application. For example, most conventional beamline experiments, including the experiment of small-angle scattering and absorption, only requires regular quality light spots. Westfahl [13] found that in the partially coherent beams of fourth-generation synchrotron radiation sources, use of mirrors with smaller errors caused wavefront distortions, but their coherence lengths were virtually unchanged. Moreover, in Church's article [2], it is also theoretically demonstrated that the imaging properties of surfaces with fractal errors perform well even if the fractal power spectrum diverges at low spatial frequencies.

In addition, how to implement the construction of such beamlines with low risk and low cost makes it necessary to carry out error evaluation of X-ray optical components for applications. With the improvement of the coherence of the light source, the application of wave optics is increasing, with the problems caused by the wave characteristics of light becoming the key to beamlines and experiments. The beamline simulation platform is important to study these problems. High-level beamline design requires a simulation platform that fully combines wave optics with traditional geometric optics tracing methods. The Ray tracing method can quickly evaluate the beamline's energy spectrum, the optics layout device's position, etc. Moreover, the existing simulation

softwares are relatively mature, such as SRW, SHADOW, XRT [14,15]. Wave optics can more accurately evaluate the changes in coherence and wavefront errors caused by various device errors and vibrations. How to quickly carry out the wave simulation of optical problems is still difficult for many researchers. To solve the problem, we will introduce our simulation strategy.

As different applications have different requirements on the image quality, Figure 1 shows the HEPs strategy on the error solution in order to give the over-/under- specification of the optics. In this paper, we studied the focusing partially coherent light and give a simplified model of the beamline system. Based on the DABAM numerical simulation, we focus on the study of the energy spatial dispersion characterization of the focused beam, and giving the general requirements for the mirror quality of the beamlines.

## Simulation methods

In order to give an explicit explanation, this paper focuses on the wavefront distortion and features of the beam spot on sample in a simplified optical system. The optical system is shown in the Figure 2, where the phase modulation function  $t(x, y) = A(x, y)e^{i\phi(x, y)}$  is used to model the X-ray optics. The simplified system setup is beneficial for improving the simulation speed and performing theoretical calculations. Numerical simulation tools have been adopted to study the issues related to the X-ray optics imperfection. It has been proved that the insert device or bending magnet can be simulated with very high precision. Optimizing the source mainly depends on the energy spectrum requirement and has little relationship with the beamline issue we are concerned about in this paper. We will perform the simulation for the specified source.

In partially coherent light sources, the wave-optics calculation of beamline simulation software is very time-consuming, which also limits its applications in the study of beamline design engineering techniques. The physical basis of the simulation is to modulate the wavefront of the light source into the detected and received data through Fresnel diffraction and to perform calculation and analysis. It can be divided into four parts: model and calculation of the light source of the insert, model of optical components, optical wave-optics propagation, and data analysis. Among them, the first and third steps are the most time-consuming processes. Figure 3 shows our strategy for the simulation platform development. In order to improve the calculation efficiency, we integrated the mature software package (XRT/SRW) and adopted the following calculation strategies:

- 1) Optimizing light source and beamline set up separately. The source field by multiple electrons is calculated and saved to the local hard disk to avoid the repeated SR source calculations, which are time-consuming. In the beamline design stage, the data is loaded and used to perform

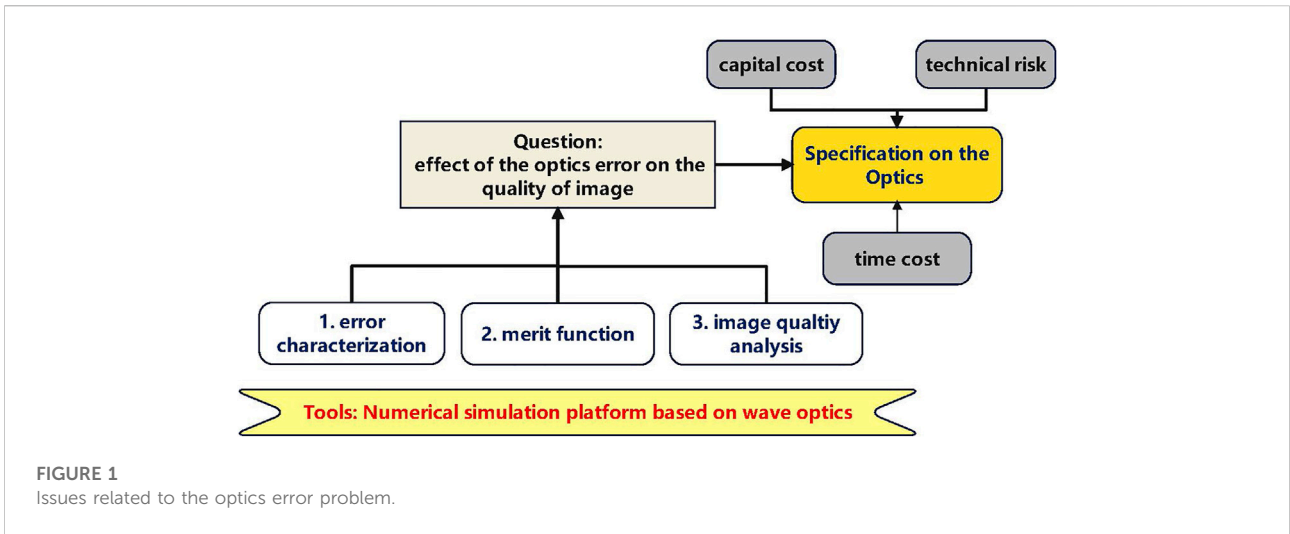


FIGURE 1 Issues related to the optics error problem.

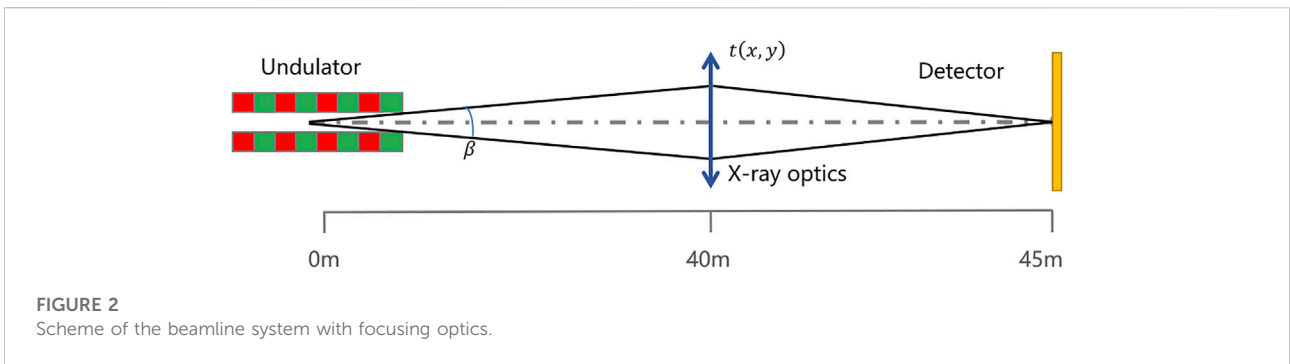


FIGURE 2 Scheme of the beamline system with focusing optics.

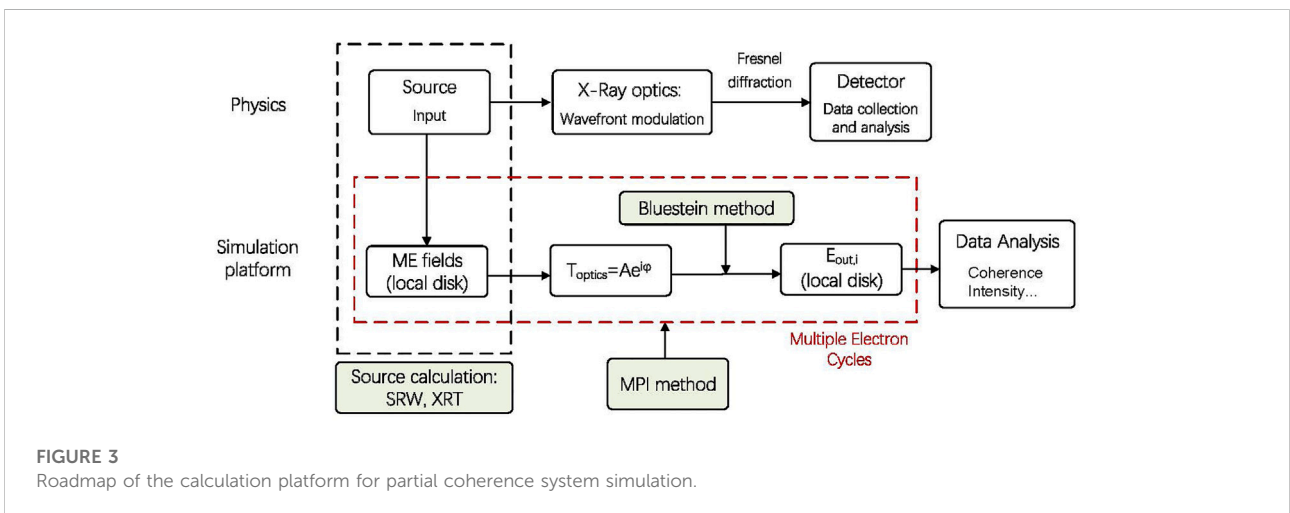


FIGURE 3 Roadmap of the calculation platform for partial coherence system simulation.

beamline simulation. Replacing numerical calculations with local data access also reduces the requirement on the large memory.

2) Optical wave propagation. Bluestein algorithm[16,17] is used to accelerate the Fresnel diffraction calculation. It can avoid the sampling issue in the traditional fast Fourier transform process.

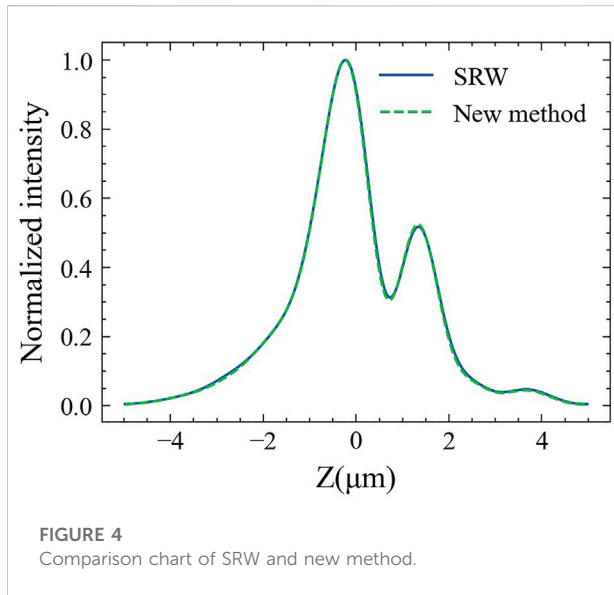


FIGURE 4 Comparison chart of SRW and new method.

TABLE 1 Parameters for the Storage and undulator.

Specification	Value
Circumference [m]	1,360
Electron energy (GeV)	6
Current (mA)	200
Electron energy spread	0.0011
Emittance horizontal/vertical [pm rad]	27.5/2.75
Horizontal/vertical size [μm]	8.8/2.3
Horizontal/vertical diver. [μrad]	3.1/1.2
Undulator	
period [mm]	16.8
number	175

TABLE 2 Parameters of X-ray light source at 10 keV for low beta beamline.

	x	z
Single electron radiation size [μm]	4.310	
Single electron radiation divergence [μrad]	5.636	
Source size [μm]	9.818	4.918
Source divergence [μrad]	6.320	5.636

3) MPI-based[18] parallel calculation for multiple electron loop. It has been successfully adopted in SRW.

Through these three optimization, this project’s calculation time is significantly reduced. In modeling the optical element, the optical element error directly converts into wavefront error. Figure 4 shows the comparison of the SRW and our method

in multi-electron simulation. The parameters of the undulator and X-ray light source are given by Table1, 2. In the debug process, the beamline parameters optimization (including sampling range, resolution, etc.) is suggested to be first carried out for single-electron calculation. After the debugging is completed, the multi-electron calculation is finally carried out.

## Surface error analysis

### Characterization of the surface error

Reasonable specification on the x-ray mirror quality should consider the features of the error data for real mirrors. In Church & Takacs [19] article, the specification of mirrors is studied based on their performance in the optical system. The Strehl Ratio (SR) and the power spectral density (PSD) of the mirror’s surface error, is selected as a merit function of image quality. Because the PSD curve changes significantly with different mirrors, the RMS slope error, RMS height error, and PV height error are commonly used to specify the optics. The surface error statistical data (1D) is obtained from the DABAM database. By subtracting the original shape of mirrors, we extracted residual height and slope error.

As shown in the Figure 5, the raw data of height error (Figure 5A), slope error (Figure 5B) and the PSD (Figure 5C) of mirror M2 from DABAM database is displayed as an example with the coordinates of Figure 5C expressed in logarithmic form.

$$\sigma(f_{max}) = \sqrt{\int_{f_{min}}^{f_{max}} psd(f)df} \tag{1}$$

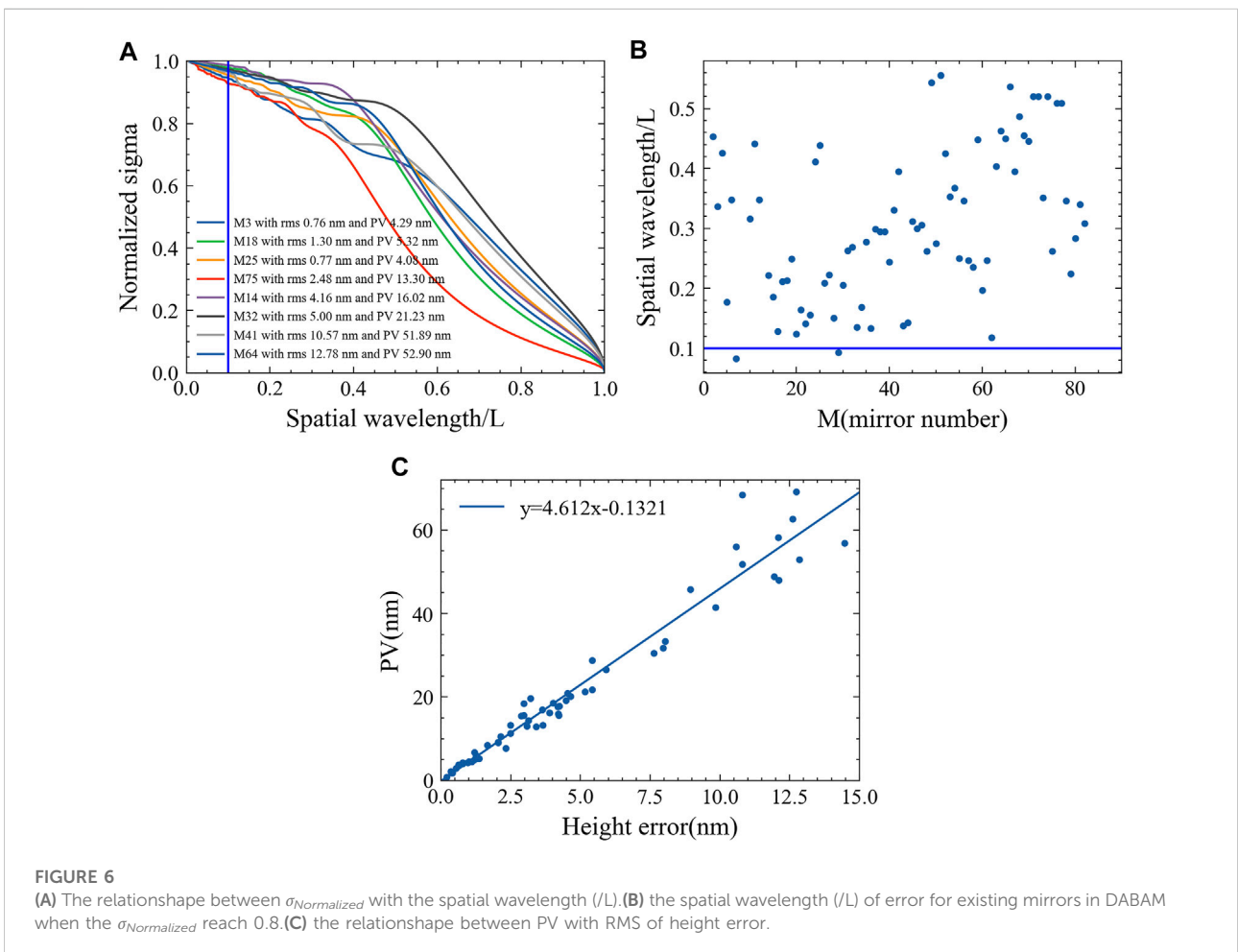
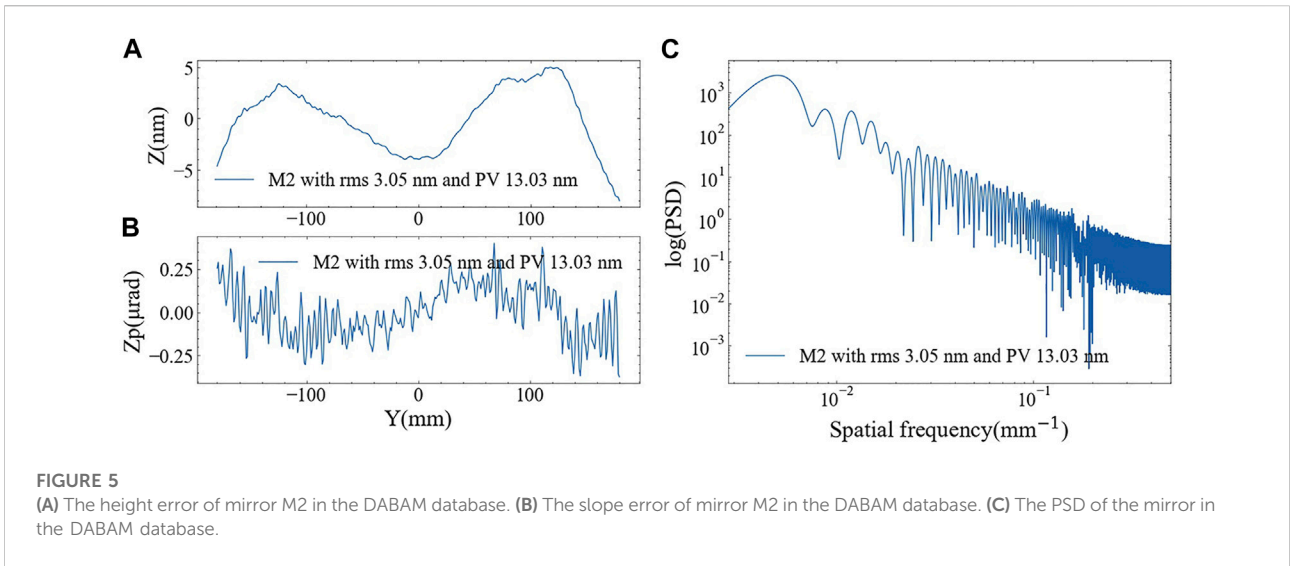
$$\sigma_{Normalized}(f_{max}) = \sigma(f_{max}) / \max(\sigma(f)) \tag{2}$$

Where there are equal interval  $df$  between sampling frequencies during the frequency range  $f_{min} = \frac{1}{L}$ ,  $f_{max} = \frac{1}{2df}$ , with  $L$  the length of the mirror,  $dy$  the spatial interval between sampling points.

Figure 6 shows the  $\sigma(f_m)$  calculated for the mirrors in the DABAM database. The  $\sigma_{Normalized}$  values exceed 0.8 when the horizontal coordinate is 0.1 for all of the mirrors, which means that low-frequency error accounts for the major component of the total error. Further, we calculate the position  $f_m$  where the  $\sigma_{Normalized}$  value reaches 0.8, the results are shown in Figure 6B demonstrating that the wavelength of the corresponding shape error is mostly greater than  $0.1L$ . Figure 6) shows the relationship between PV and RMS of height error is approximately linear, which simplifies the analysis procedure later.

## Deterministic analysis on the beamline performance

From the point of view of integration calculation, it is challenging to perform an analytical analysis of the low-frequency error. However, the physical rules behind the



appearance are more important for practical beamline design work than simulation. In Section 2.2, it can be seen that the low-frequency error is the main component of the machining error. In order to study the influence of the spatial distribution characteristics of the surface shape error on the optical system performance, considering the statistical dilemma, here we develop the deterministic analysis method. In the case of a coherent light field, the entire aperture function  $t(x_1)$  is divided into many segments, and the transmittance function in each segment can be expressed as

$$t_i(x_1) = \text{rect}\left(\frac{x_1 - c_i}{w_i}\right) f_i(x_1) \tag{3}$$

Where  $w_i$  and  $c_i$  are segment width and center position.  $f_i(x_i) = \exp[-j\frac{4\pi h(x_i)\sin\theta}{\lambda}]$  is error distribution function.  $\text{rect}(\dots)$  is the rectangular function. It is easy to obtain the light field distribution on the focal plane as

$$U(x_0, y_0) = \frac{e^{jkz} e^{jk\frac{(x_0^2+y_0^2)}{2z}}}{j\lambda z} \mathcal{F}[U(x_1, y_1)]|_{f_x=\frac{x_0}{\lambda z}, f_y=\frac{y_0}{\lambda z}}$$

$$= C \sum_i \exp(-j2\pi f_x c_i) [w_i \text{sinc}(w_i f_x)] * \mathcal{F}[f_i(x_i)]|_{f_x=\frac{x_0}{\lambda z}} \tag{4}$$

Where  $x_0$  and  $y_0$  are the coordinates of the focal plane,  $x_1$  and  $y_1$  are the coordinates of aperture,  $k$  is the wave number,  $z$  is the distance to the focal plane,  $\mathcal{F}[\dots]$  is the Fourier transform function,  $f_x$  is spatial frequency in the x-direction, and  $C$  is a constant. The intensity of the light field is given by

$$I(x_0, y_0) = U^*(x_0, y_0)U(x_0, y_0) \tag{5}$$

According to the Formulas 4 and 5, the final light field distribution can be divided into three contributions: [a]. Single slit diffraction factor  $w_i \text{sinc}(w_i f_x)$ . Slit width determines peak intensity and distribution width. [b]. Positional parameters  $\exp(-2\pi f_x c_i)$  is the phase factor due to distance between slits. [c]. Diffraction modulation within each single hole  $\mathcal{F}[f_i(x_1)]|_{f_x=\frac{x_0}{\lambda z}}$ . Consider the Cosine model, we have  $f_i(x_1) = \exp[j\frac{m}{2} \cos(2\pi f_0 x_1)]$  and the Fourier transform function is

$$\mathcal{F}[f_i(x_1)]|_{f_x=\frac{x_0}{\lambda z}} = \sum_{q=-\infty}^{\infty} (j)^q J_q\left(\frac{m}{2}\right) \delta(f_x - qf_0, f_y) \tag{6}$$

$J_q(\frac{m}{2})$  is  $q$ -order Bessel function of the first kind,  $f_x$  is initial frequency. Each level component is shown in the Figure 7. Only the finite level can be considered when the error level is relatively low. As the height error increases, the higher-order contribution increases, leading to a dispersion of the light field over a large angular range. For general smooth surfaces, choosing the 0 and  $\pm 1$  order spreads of the Cosine wave is sufficient.

To demonstrate the effectiveness of this approach, Figure 8 presents the results of the piecewise approximation of the shape error under parallel light illumination for Mirror-34 from the DABAM database. It is shown that the piecewise approximation can generate the profile of the light field similar to the result by

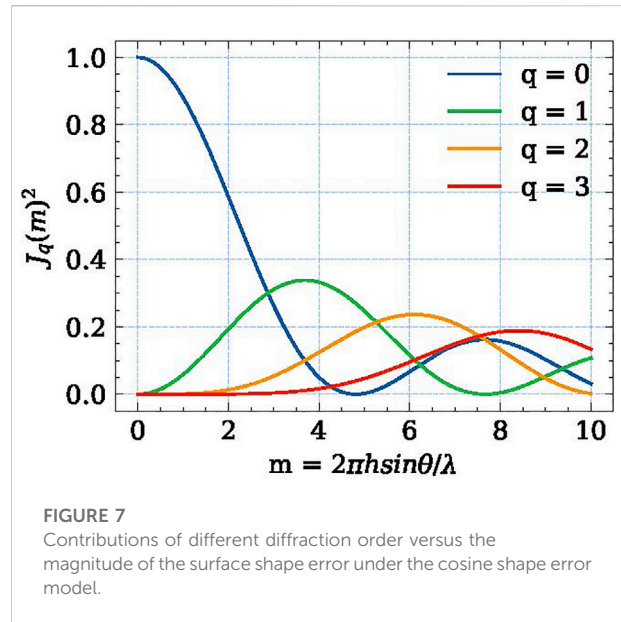


FIGURE 7 Contributions of different diffraction order versus the magnitude of the surface shape error under the cosine shape error model.

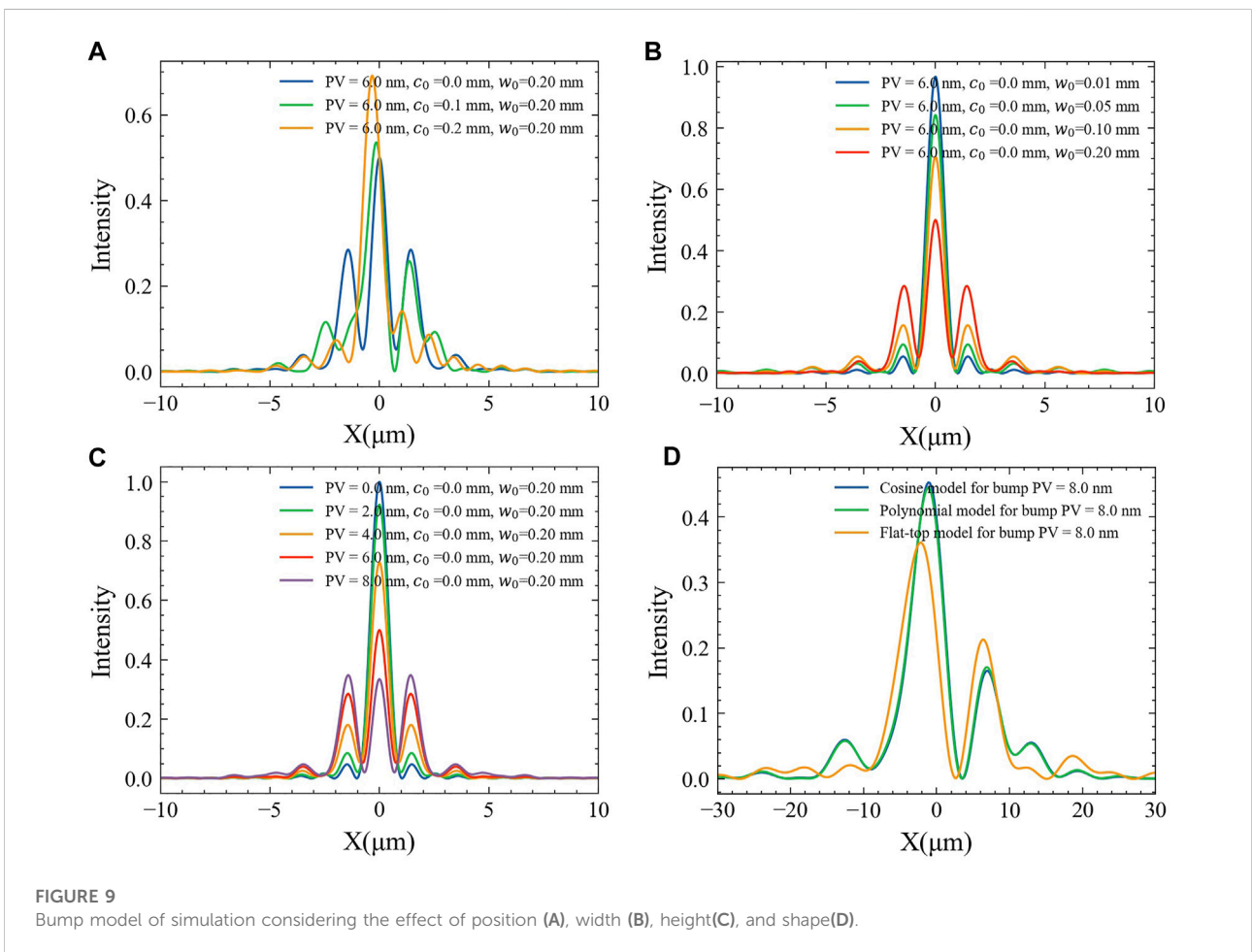
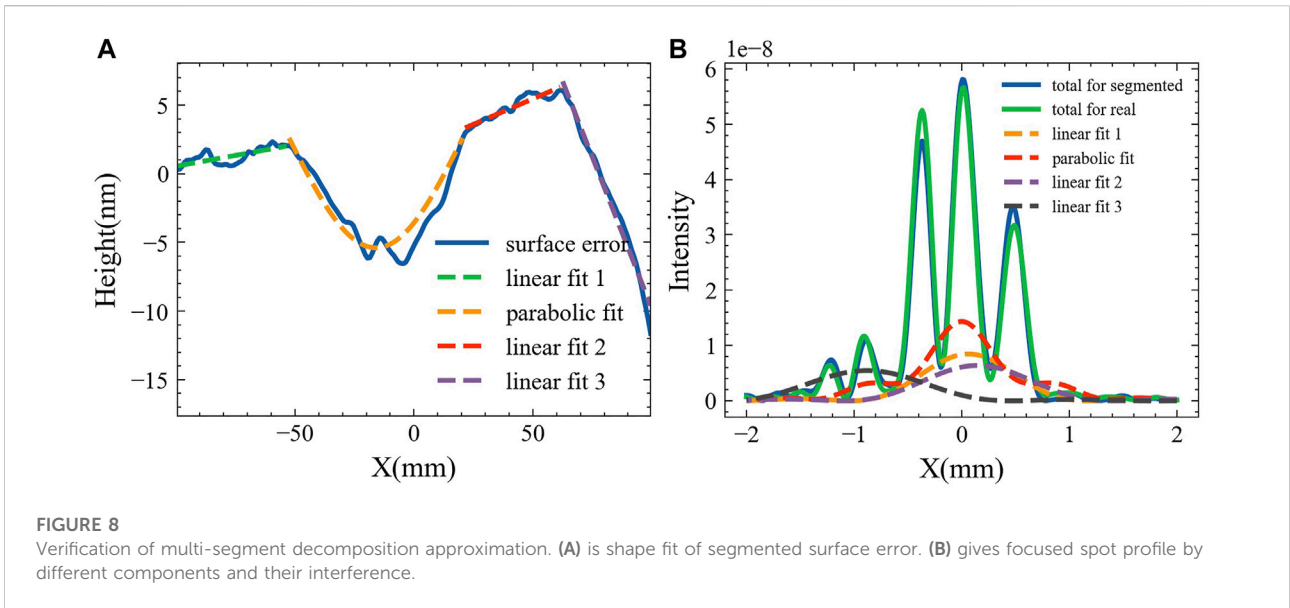
the nature error. It also verifies that the low-frequency error contributes to the structure in the focal spot. The structure feature can be well analyzed by a deterministic method using the segmented model with simple functions.

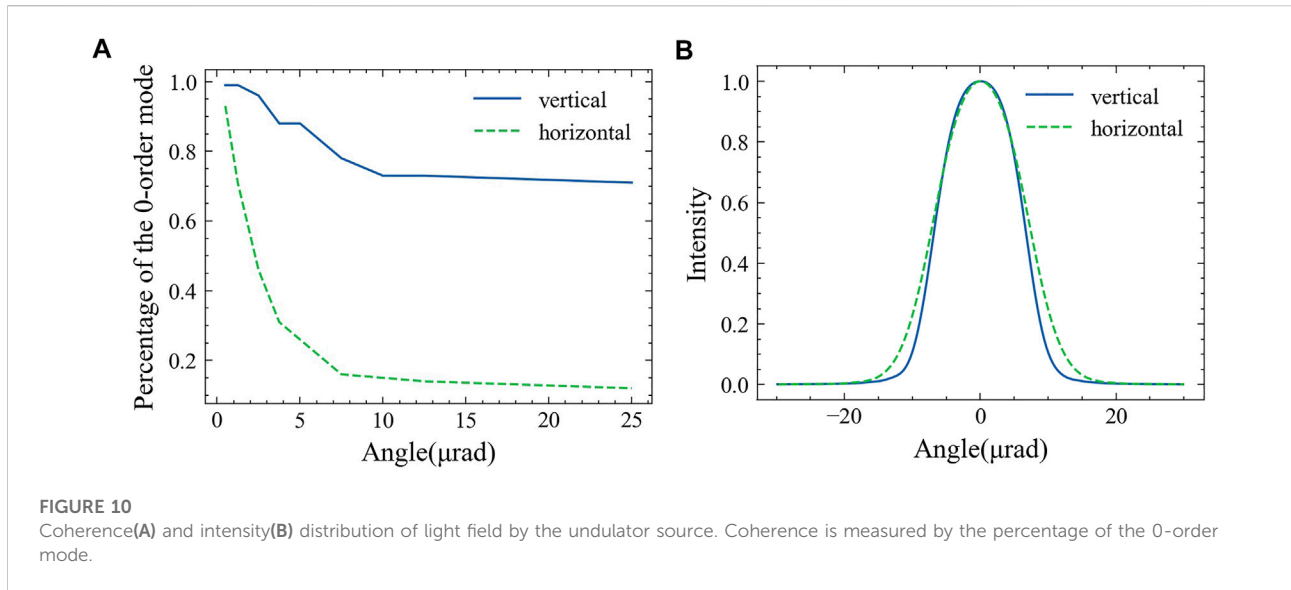
On the other hand, quantitatively, the simplest single-bump case can be considered to analyze the impact of low-frequency errors. The bump is set in the middle of the section. The width of the bump is  $w_0$ , the center position  $c_0$ , and the width of the entire aperture of the amplitude PV is  $w$ .

In the case of complete coherence, the distribution of the light spot on the focal plane is shown in the Figure 9 when considering the effect of position, width, height, and shape. The bump's position will cause the symmetry of the light field distribution, and the width will cause the intensity distribution of the interference fringes. The smaller the width of the bump, the smaller the error contribution of this part. As the height of the bump changes, multiple cycles of wavefront oscillations are formed in the bump, which also causes structural changes. Although the cosine distribution model is used in the above calculation, it does not affect the conclusion of the light field distribution structure compared with the calculation results of the parabolic and flat-topped model.

## Merit function selection

In this section, we perform error experiments in a low-beta beamline of the HEPS light source. The parameters of the HEPS storage ring and the insert device are shown in Table 1, and the corresponding light source parameters are shown in Table 2. The Figure 10 uses the beamline tracing and mode decomposition modules to calculate the coherence and the angular distribution





of the light field in different angular ranges. The source can provide X-ray with perfect coherence in the vertical direction, and the coherence ratio in the horizontal direction is less than 20%. The focusing characteristics in these two directions can reflect the relationship between the degree of coherence and error characteristics. At the same time, considering the efficiency of the optical field flux, the acceptance angle range to be studied in this paper is 10  $\mu\text{rad}$  in the vertical direction and 18  $\mu\text{rad}$  in the horizontal direction.

### Strehl ratio

SR is the illuminance ratio at the center of the system’s Airy disk to the comparable value in an ideal imaging system. It is widely used as a standard function for diffraction limited systems. SR shows the degree of energy dispersion, the effect of diffraction and aberrations on the Airy disk. When SR is above 0.8, it is usually dependable in most optical system. The closer SR approaches to 1, the better the imaging quality are.

The relationship between the RMS optical path difference  $W_{rms}$  and SR is

$$D_s = e^{-(2\pi \frac{W_{rms}}{\lambda})^2} = e^{-(2\pi \frac{h \sin \theta}{\lambda})^2}$$

Where  $h$  is height of mirror. The aberration is relatively modest for  $SR > 0.8$ , and the SR can be approximated as

$$D_s = 1 - (2\pi)^2 \left(\frac{W_{rms}}{\lambda}\right)^2 \tag{7}$$

The surface error in the DABAM library is added on the horizontal and vertical directions in our simulation process, respectively. In the numerical experiment, the residual shape

error is added on the vertical direction for the beamline acceptance angle  $\beta = 10 \mu\text{rad}$  and on the horizontal direction for  $\beta = 18 \mu\text{rad}$ , which corresponds to the different coherence of the light field. Figure 11 is the SR of simulation in which we calculate the theoretical value of SR and the RMS height error using the Formula 7. SR scatter plots for 10  $\mu\text{rad}$  and 18  $\mu\text{rad}$  receive angles in response to height error are shown in Figure 11A,B. When 1) and 2) are compared, it is clear that the 10  $\mu\text{rad}$  results differ from the 18  $\mu\text{rad}$  results. The 10  $\mu\text{rad}$  results are more associated in theory than 18  $\mu\text{rad}$  results. This demonstrates that, in good coherence, especially more than 0.8, the theoretical value of SR related to the height error can be utilized as a mirror selection criterion. We also noticed that the correlation between the theoretical and actual values reduces when the SR drops. Figure 11C,D give scatter plots of slope error versus SR value, which do not show a clear correlation between them. The above results show that the SR value can describe the dispersion degree of the light field only in the system close to the diffraction limit. SR is closely related to the height error.

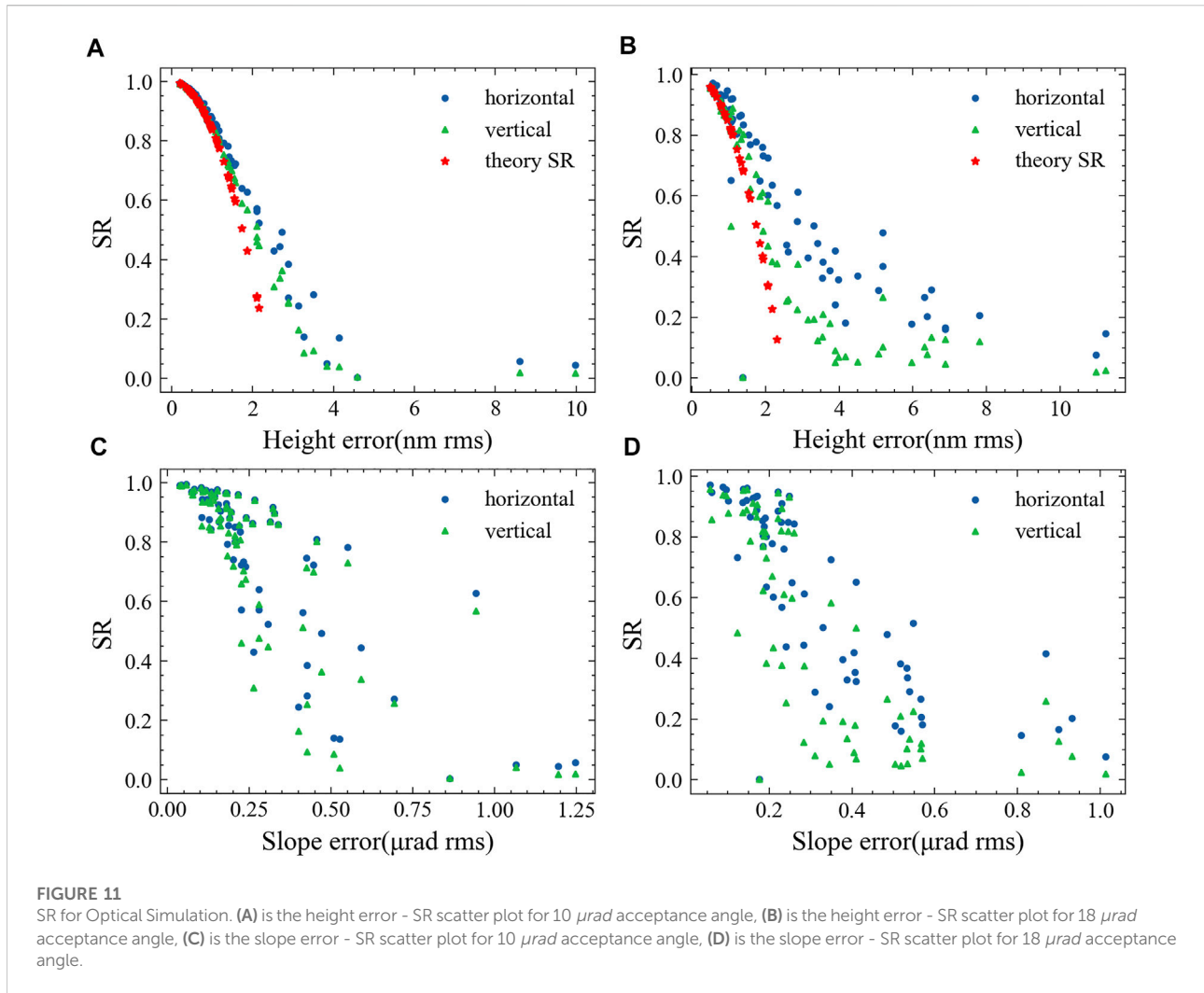
### Root-mean-square spot size

The extension of the spot is another measure of the energy or flux spread caused by the error. It should consider three contributions, including diffraction, geometric magnification, and the surface error given by

$$D_{geometry} = \sigma_{source} M \tag{8}$$

$$D_{Airy} = C \frac{2\lambda}{D} q \tag{9}$$

$$D_{error} = 2q\sigma_{slope} \sin \theta \tag{10}$$

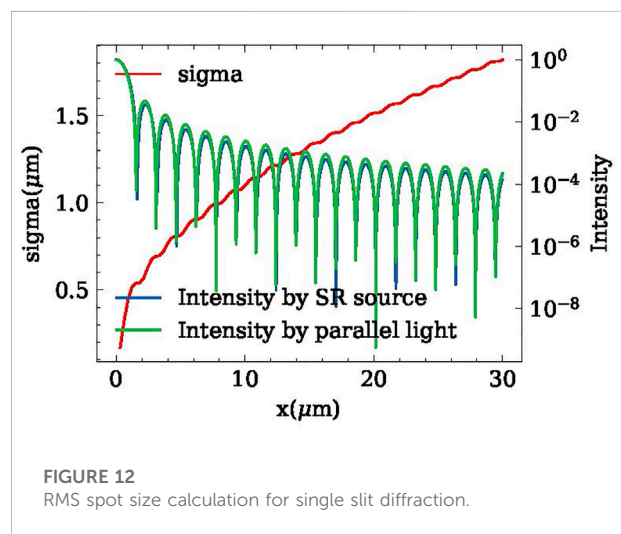


where  $M = \frac{q}{p} = \frac{1}{8}$ ,  $q$  is image distance and  $p$  is object distance.  $C$  is a constant,  $D$  is aperture diameter,  $\sigma_{slope}$  is the residual surface error and  $\theta$  is the gracing angle. The convolution of the three parts will all contribute to the final spot width:

$$D_{total} = (D_{source}^2 + D_{error}^2 + D_{Airy}^2)^{1/2} \quad (11)$$

For single slit diffraction, the distribution of the light field is  $I(t) = \text{sinc}(t)^2$ ,  $t = \frac{\pi D \sin \theta}{\lambda} = \frac{\pi D x}{\lambda f}$ . We pay attention to the positions of the first minimum  $t_{1,min} = \pm\pi$ . The position of half width is at  $t_{FWHM} = \pm 1.39$ , thus the FWHM is  $x = 0.88 \frac{\lambda f}{D}$ . If the transformation relationship of 2.35 times between FWHM and sigma is defined according to the Gaussian distribution, there is a relationship of  $\sigma_{spot} = 0.37 \frac{\lambda f}{D}$ . From the distribution of the real light field, the RMS size of the light field size is given by

$$\sigma_{spot}^2 = \frac{\int I(t) t^2 dt}{\int I(t) dt}$$



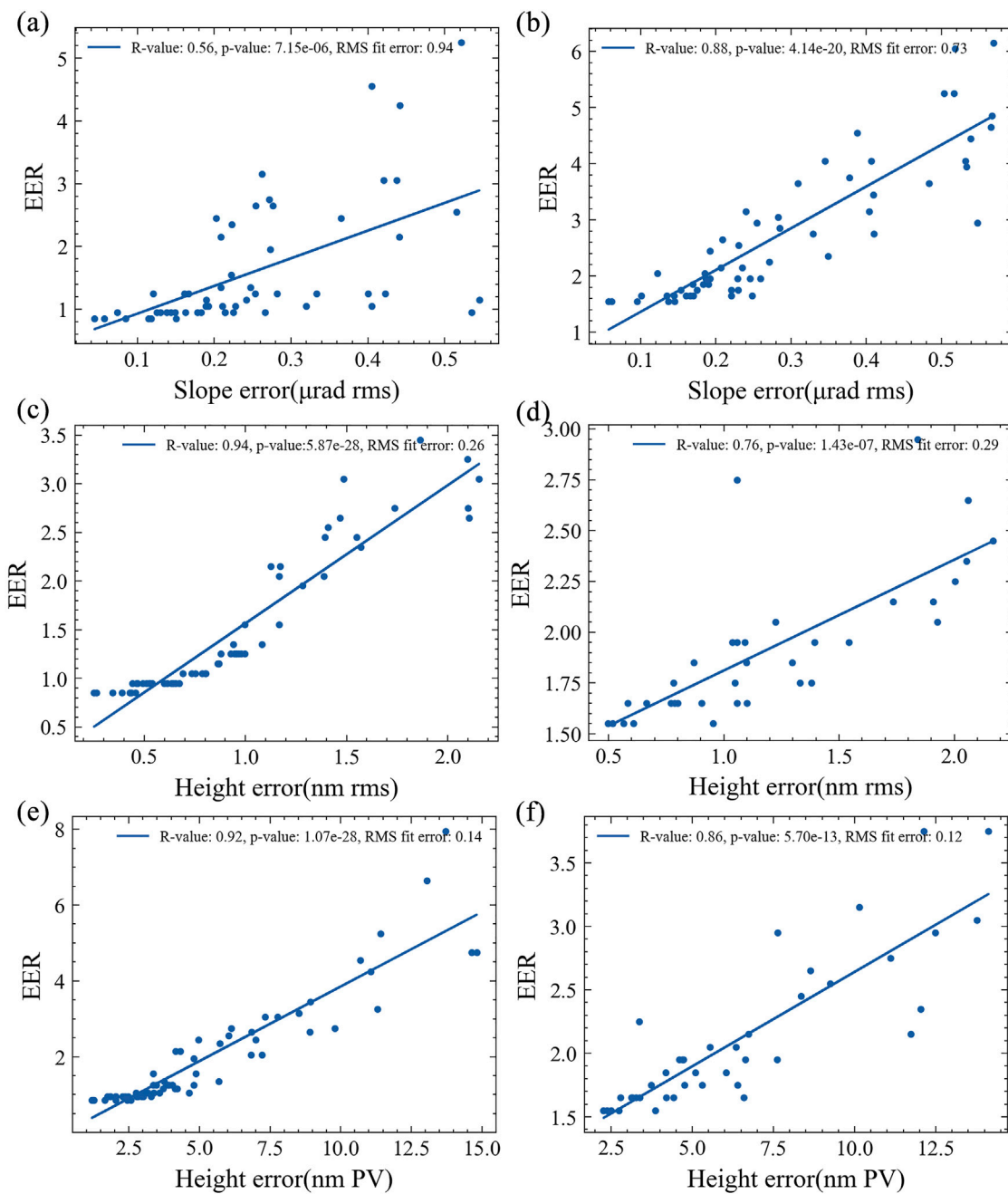


**FIGURE 13**  
 Encircled energy spot radius by values of RMS slope error(A,B), RMS height error(C,D) and PV height error(E,F). The left and right columns correspond to 10  $\mu rad$  acceptance angle in vertical direction and 18  $\mu rad$  acceptance angle in horizontal direction, respectively. The criterion for the encircled energy spot radius width is 70%.

The value of the integral spot size fluctuates with the range of the light field using this connection. We get  $\sigma_{spot} = 0.4 \frac{\lambda f}{D}$  for single slit diffraction if we limit it to the first principal maximum range, which is very close to the Gaussian assumption.

Then, we calculate the light SR field diffracted by the single slit, where the selected acceptance angle is 10  $\mu rad$ . In the

Figure 12, the first integral width sigma value is 0.538  $\mu m$ , the minimum position is 1.593  $\mu m$ , and the ratio is 0.538/1.593 = 0.33. It is consistent with the theoretical slit diffraction width characteristics. However, the integrated sigma value will increase significantly with the increase of the integration range. For example, the sigma value in this calculation is 1.8  $\mu m$  over  $\pm$

30  $\mu\text{m}$ . In practical applications, the experiment will configure a slit to block weak light from a large angle while only maintaining intense light in the central lobe, which already holds 90% of the light field energy and ensures a higher system spatial resolution at the same time. Unlike a Gaussian distribution, the spot's standard deviation size cannot accurately reflect the spot's energy dispersion in advanced light sources. As a result, we suggest that it is unsuitable for use as a light field standard.

## Encircled energy radius

Encircled energy is another metric for specifying the performance of traditional optical systems, which is defined as the flux in a circle as a function of radius. However, it has not yet been studied and used in the SR beamline design. In this section, we will demonstrate that this metric is good for the spatial dispersion of the light field considering different coherence. The encircled energy distribution is calculated by integrating intensity from the center. When no specular error is loaded, the flux obtained by taking the FWHM of the intensity curve of focal plane as the encircling radius which is 70.6% for vertical direction and 72.2% for horizontal direction. And the ratio of the flux at the FWHM of the standard Gaussian distribution is 76%. Therefore, we calculated 76% flux of encircling energy radius.

In Figure 13, 76% encircled energy radius of the focus spot is plotted versus different surface error parameters with a linear regression fit performed. Figure 13B shows a more significant Pearson correlation coefficient and a smaller  $p$ -value for the hypothesis test compared to Figure 13A, indicating that the coordinate value of 18  $\mu\text{rad}$  with 76% light intensity is more correlated with the slope error. Similarly, compared to Figure 13D, Figure 13C has a more significant Pearson correlation coefficient and a smaller  $p$ -value for the hypothesis test, indicating that the coordinate value of 10  $\mu\text{rad}$  containing 76% of the light intensity is more correlated with the height error. This finding is similar to the result by Church & Takacs [19] that the performance is related to the height error for the coherent system while to the slope error for the low-coherence system. In addition, the PV and RMS height errors have shown no significant difference in the encircled energy radius in both cases, suggesting that both can be used to specify the mirror quality.

## Conclusions

The influence of X-ray mirror error on beamline system performance is studied in this paper. We employ a simplified model and an accelerated simulation platform with improved computational efficiency for error analysis. It is investigated through the analysis of error characteristics and the

simulation of beamline performance in order to identify more effective specification methods for various applications. As a result, we arrive at the following conclusion:

- 1) While the statistics of individual mirrors are highly debatable, the RMS and PV height error can be used together to constrain mirror errors. Low-frequency component with a period greater than  $1/10 L$  is the major contributor to the fabrication error.
- 2) It is required to reduce the residual surface error to get an unstructured light spot. We discovered that a low-frequency mistake of more than  $1/10 L$  period impacts system performance through the deterministic analysis and bump simulation.
- 3) The encircled energy spot size is a good measure for spatial energy dispersion for partial coherence application.

Through the calculation and analysis in this paper, it is helpful to determine the parameter requirements of low-risk optical components. On the other hand, the calculation method in this paper can also be used to study other problems, such as vibration, coherence control, and others, which require many wave calculations. In addition, some adaptive X-ray mirrors have been reported to control and correct low-frequency defects [20,21], and we hope to investigate such mirrors in the future.

## Data availability statement

The raw data supporting the conclusions of this article will be made available by the authors, without undue reservation.

## Author contributions

WS: taking part in the improvement on the paper work. QJ: calculation and discussion on the error feature. WZ: added frames and contents.

## Funding

Youth Innovation Promotion Association of the Chinese Academy of Sciences (2019012); National Natural Science Foundation of China (11875059).

## Conflict of interest

The authors declare that the research was conducted in the absence of any commercial or financial relationships that could be construed as a potential conflict of interest.

## Publisher's note

All claims expressed in this article are solely those of the authors and do not necessarily represent those of their affiliated

organizations, or those of the publisher, the editors and the reviewers. Any product that may be evaluated in this article, or claim that may be made by its manufacturer, is not guaranteed or endorsed by the publisher.

## References

- Jiao Y, Xu G, Cui X-H, Duan Z, Guo Y-Y, He P, et al. The heps project. *J Synchrotron Radiat* (2018) 25:1611–8. doi:10.1107/s1600577518012110
- Church EL, Takacs PZ. Specification of surface figure and finish in terms of system performance. *Appl Opt* (1993) 32:3344–53. doi:10.1364/ao.32.003344
- Signorato R, del Rio MS. Structured slope errors on real x-ray mirrors: Ray tracing versus experiment. In: *Materials, manufacturing, and measurement for synchrotron radiation mirrors*, 3152. Washington, United States: International Society for Optics and Photonics (1997). p. 136–47.
- Pardini T, Cocco D, Hau-Riege SP. Effect of slope errors on the performance of mirrors for x-ray free electron laser applications. *Opt Express* (2015) 23:31889–95. doi:10.1364/oe.23.031889
- Yashchuk VV, Samoylova L, Kozhevnikov IV. Specification of x-ray mirrors in terms of system performance: A new twist to an old plot. In: *Advances in computational methods for X-ray optics III*, 9209. Washington, United States: SPIE (2014). p. 114–32.
- Shi X, Assoufid L, Reininger R. How to specify super-smooth mirrors: Simulation studies on nano-focusing and wavefront preserving x-ray mirrors for next-generation light sources. In: 8th International Symposium on Advanced Optical Manufacturing and Testing Technologies: Subnanometer Accuracy Measurement for Synchrotron Optics and X-Ray Optics, 25 October, 2016, Suzhou, China, 9687. SPIE (2016). 9–19.
- Church EL, Takacs PZ. Optimal estimation of finish parameters. *Opt Scatter: Appl Meas Theor*, 1530. Washington, United States: International Society for Optics and Photonics (1991). p. 71–85.
- Yashchuk YV, Yashchuk VV. Reliable before-fabrication forecasting of expected surface slope distributions for x-ray optics. *Opt Eng* (2012) 51:046501. doi:10.1117/1.oe.51.4.046501
- Church EL. Fractal surface finish. *Appl Opt* (1988) 27:1518–26. doi:10.1364/ao.27.001518
- Church EL, Takacs PZ. Instrumental effects in surface finish measurement. In: *Surface measurement and characterization*, 1009. Washington, United States: International Society for Optics and Photonics (1989). p. 46–55.
- Krywka C, Last A, Marschall F, Márkus O, Georgi S, Müller M, et al. Polymer compound refractive lenses for hard x-ray nanofocusing. In: AIP Conference Proceedings, 30 August, 2016, Upton, NY, USA, 1764. AIP Publishing LLC (2016). p. 020001.
- Mimura H, Takei Y, Kume T, Takeo Y, Motoyama H, Egawa S, et al. Fabrication of a precise ellipsoidal mirror for soft x-ray nanofocusing. *Rev Scientific Instr* (2018) 89:093104. doi:10.1063/1.5035323
- Westfahl H, Jr, Lordano Luiz SA, Meyer BC, Meneau F. The coherent radiation fraction of low-emittance synchrotrons. *J Synchrotron Radiat* (2017) 24:566–75. doi:10.1107/s1600577517003058
- Klementiev K, Chernikov R. Powerful scriptable ray tracing package xrt. In: *Advances in computational methods for X-ray optics III*, 9209. Washington, United States: SPIE (2014). p. 60–75.
- Chubar O, Elleaume P. Accurate and efficient computation of synchrotron radiation in the near field region. In: proc. of the EPAC98 Conference; 22–26 June 1998; Stockholm, Sweden, 1177 (1998).
- Bluestein L. A linear filtering approach to the computation of discrete fourier transform. *IEEE Trans Audio Electroacoust* (1970) 18:451–5. doi:10.1109/tau.1970.1162132
- Hu Y, Wang Z, Wang X, Ji S, Zhang C, Li J, et al. Efficient full-path optical calculation of scalar and vector diffraction using the bluestein method. *Light Sci Appl* (2020) 9:119–1. doi:10.1038/s41377-020-00362-z
- Dalcin L, Fang Y-LL. Mpi4py: Status update after 12 years of development. *Comput Sci Eng* (2021) 23:47–54. doi:10.1109/mcse.2021.3083216
- Church EL, Takacs PZ. Specification of glancing-and normal-incidence x-ray mirrors [also erratum 34 (11) 3348 (nov1995)]. *Opt Eng* (1995) 34:353–60. doi:10.1117/12.196057
- Signorato R, Hignette O, Goulon J. Multi-segmented piezoelectric mirrors as active/adaptive optics components. *J Synchrotron Radiat* (1998) 5:797–800. doi:10.1107/s0909049597012843
- Goto T, Matsuyama S, Hayashi H, Yamaguchi H, Sonoyama J, Akiyama K, et al. Nearly diffraction-limited hard x-ray line focusing with hybrid adaptive x-ray mirror based on mechanical and piezo-driven deformation. *Opt Express* (2018) 26:17477–86. doi:10.1364/oe.26.017477